Structure and Rheology of Aramid Solutions: Transient Rheological and Rheooptical Measurements

S. J. Picken,* J. Aerts, H. L. Doppert, A. J. Reuvers, and M. G. Northolt

Akzo Research Laboratories Arnhem, Corporate Research, Physical Chemistry Department, P.O. Box 9300, 6800 SB Arnhem, The Netherlands

Received May 7, 1990; Revised Manuscript Received June 15, 1990

ABSTRACT: Some results are presented on the rheology of the lyotropic nematic phase of the aramid polymers poly(*p*-phenyleneterephthalamide) and poly(4,4'-benzanilidyleneterephthalamide) in concentrated sulfuric acid. Controlled-stress and controlled-strain rheometry, polarization microscopy, conoscopy, and synchrotron X-ray scattering were used to study the change in the structure of the solutions during the start-up of simple shear flow. The experimental results are discussed in terms of a qualitative model for the structure of these solutions. The development of orientation during the start-up of flow is explained by using an affine deformation model.

Introduction

We present some results on the rheology of the lyotropic nematic phase of fully aromatic polyamides in concentrated sulfuric acid. The aramid polymers that were used are shown in Figure 1. An anisotropic nematic phase is found above ca. 10% (w/w) concentration of these polymers. At lower concentrations and ambient temperature an isotropic solution is found. Here we give some results on 19.8% (w/w) solutions of poly(*p*-phenyleneterephthalamide) (PPTA) and poly(4,4'-benzanilidyleneterephthalamide) (DABT). The DABT solutions are used as a model system, as they do not form a crystal–solvate phase at high polymer concentration. This has the advantage that the rheology of DABT solutions of 19.8% (w/w) can be studied at room temperature. PPTA solutions of this concentration melt at ca. 60 °C.

In Figure 2 we show the local molecular structure in these solutions; the wormlike molecules are oriented on average along the local orientation axis or director $\tilde{n}$. The degree of molecular orientation with respect to $\tilde{n}$ is described by the orientational distribution function $f(\beta)$. In the solutions studied here $f(\beta)$ is a sharply peaked distribution (about angles 0 and π) and is approximately given by a Gaussian function. This local orientational order is an intrinsic property of the solution: $f(\beta)$ is determined by the thermodynamics of the solutions and thus by the temperature T, the polymer concentration c, and the average molecular weight $\bar{M}_w$.[1-3]

In addition to this local orientational order we have to consider the macroscopic orientational order of the director field $\tilde{n}(\mathbf{r})$. The director orientation is, in general, influenced by external fields such as electric, magnetic, and/or shear and elongational flow fields. It will be clear that the influence of flow fields on the degree of director orientation or the texture of the sample is of fundamental importance, e.g., for understanding the aramid fiber-spinning process.

A general review of the rheology of lyotropic main-chain polymers has been given by Berry.[4] Here we discuss some of the structural changes in aramid solutions during the start-up of simple shear flow.

Experimental Results

A variety of transient rheological methods have been used to study aramid solutions. It is of interest to study the transient behavior, as the structure of the aramid solutions changes dramatically due to the applied deformation. The aramid solutions used in the experiments

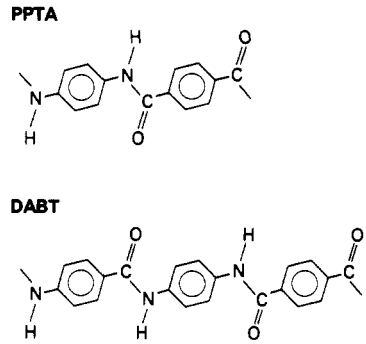

Figure 1. The aramid polymers: poly(*p*-phenyleneterephthalamide) (PPTA) and poly(4,4'-benzanilidyleneterephthalamide) (DABT).

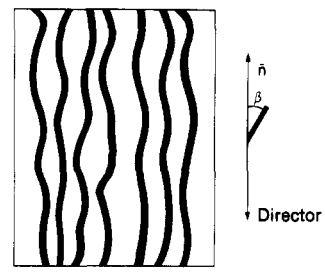

Figure 2. Local structure in the lyotropic nematic phase.

were either PPTA or DABT solutions of 19.8% (w/w) in 99.8% H_2SO_4. The molecular weight value $\bar{M}_w$ was ca. 30 000 for both samples. This value was obtained by using a calibration curve relating the viscosity of a dilute solution to the $\bar{M}_w$ value obtained by various methods, e.g., GPC, end-group analysis, and SALS. Where necessary the aramid solutions were protected against coagulation (by ambient moisture) by flushing the rheometer with dry nitrogen gas. The actual occurrence of coagulation can be easily observed by a change in the color of the sample.

(i) Transient Shear Stress Experiments.[5] Using a Contraves Rheomat 135S rheometer (Couette geometry) we have studied the transient shear stress. In a transient shear stress experiment a constant shear rate is applied at time t_0 and the resulting shear stress is measured as a function of time. At time t_s the shear flow is stopped and the stress relaxation can be measured. In Figure 3 we schematically show the shear rate and shear stress as a function of time. We will not consider the stress relaxation process further but will focus on the start-up behavior.

In Figure 4 we show the transient response of the reduced

0024-9297/91/2224-1366$02.50/0

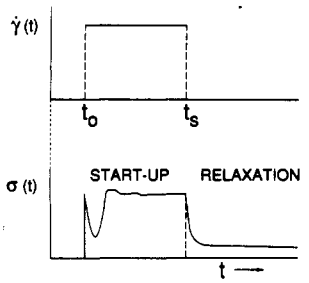

Figure 3. Shear rate $\dot{\gamma}(t)$ and shear stress $\sigma(t)$ during a transient shear stress measurement.

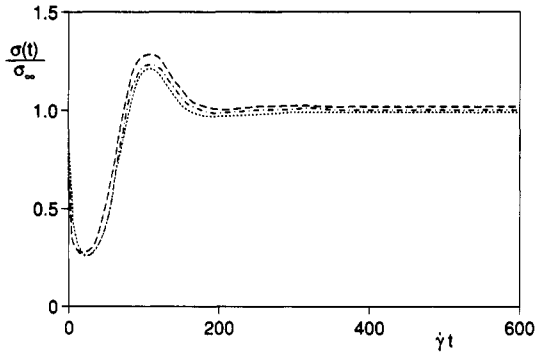

Figure 4. Reduced transient shear stress as a function of $\dot{\gamma}t$, the applied strain (19.8% (w/w) PPTA, 80 °C) for three shear rates $\dot{\gamma}$ 1 (– – –), 2 (• – •), and 4 (•••) s^{-1}.

shear stress $\sigma(t)/\sigma_\infty$ as a function of shear strain, as given by $\dot{\gamma}t$, for three shear rates $\dot{\gamma}$ (1, 2, and 4 s^{-1}). At the start of the transient shear stress the solution has a reproducible initial structure; i.e., we have waited for a long time since the last deformation of the sample. In practice, a rest time of about 10 min appears to be sufficient to obtain a reproducible initial structure. From Figure 4 it is observed that the reduced shear stress shows a remarkable oscillatory behavior, only reaching the steady-state value σ_∞ after a relatively long time. The large-strain steady-state shear stress σ_∞ can be described reasonably well by a power-law type of equation:

$$\sigma_\infty = K\dot{\gamma}^\alpha \tag{1}$$

with K = 166 Pa and α = 0.7 at 80 °C and 20% (w/w). Also, from Figure 4 it is observed that the transient of $\sigma(t)/\sigma_\infty$ is determined by the overall applied strain $\dot{\gamma}t$ since the start of the flow.

The experiments show that the transient behavior in $\sigma(t)$ is completely determined by strain and that the overall stress level is completely determined by the shear rate using eq 1. A similar decomposition has been applied to transient shear stress measurements on PBLG solutions.[6]

(ii) Recoil after Creeping Flow. During a recoil experiment a constant shear stress is applied at time t_0 and the resulting strain, the creeping flow, is recorded as a function of time. Then at time t_s and corresponding applied strain γ_a the stress is "switched off" and the resulting recoil strain of the sample is measured as a function of time. In Figure 5 we show some schematic curves for the shear stress and the shear strain as a function of time. The recovered strain $\gamma_r(\infty)$, i.e., after having waited for a long time after switching off the stress, is a measure for the "structure" in the sample at strain γ_a. The relative recovered strain $\gamma_r(\infty)/\gamma_a$ measures to what extent the sample has "forgotten its initial structure" at rest due to the application of strain γ_a.

In Figure 6 we show the results of a recoil experiment using a Carri-Med CS100 controlled-stress rheometer for

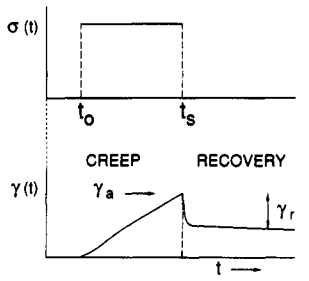

Figure 5. Shear stress $\sigma(t)$ and shear strain $\gamma(t)$ during a recoil experiment.

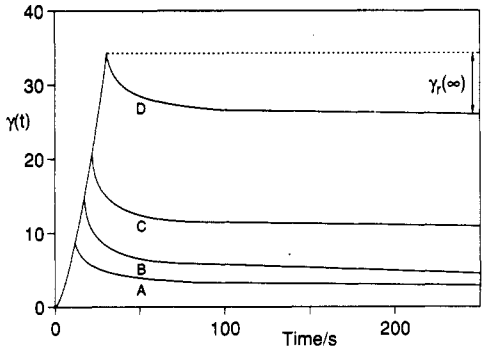

Figure 6. Recoil measurement using a controlled-stress rheometer on a 19.8% (w/w) PPTA solution at 80 °C. Stress level 125 Pa; prestrain values γ_a (A) 9, (B) 16, (C) 22, and (D) 35.

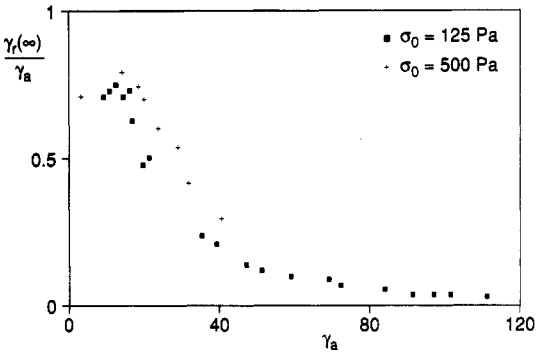

Figure 7. Relative ultimate recovered strain $\gamma_r(\infty)/\gamma_a$ as a function of the applied strain γ_a for the stress levels as indicated.

various applied strains γ_a. The ultimate recoil strain $\gamma_r(\infty)$ first increases with the applied strain and then decreases to a final value of ca. 3 for large prestrains γ_a. The value for the ultimate recoil strain $\gamma_r(\infty)$ is determined at a relaxation time of 500 s. That this is a sufficiently long time to obtain a good estimate of the final (infinite time) recovered strain was checked by using a strain versus log (t) curve.

The relative recovered strain can be used as a measure for the change in the "structure" during the creeping flow. This is shown in Figure 7 as a function of the applied strain. Although there are small differences for the two stress levels shown in Figure 7, the relative recovered strain is largely determined by the applied prestrain γ_a. It is apparent that the PPTA solution shows an enormous amount of elastic recoil for prestrain values of less than ~20. Nearly 70% of the applied strain is recovered in this range of prestrains. The largest recorded recoil strain was ~15; this should be compared to values of ~2–3 for traditional polymer melts. Above ~25 strain units the relative recovered strain decreases rapidly, so that the solution has forgotten its initial equilibrium structure before the application of the stress. For large applied strains γ_a the relative recoil strain decreases to zero proportional to $1/\gamma_a$. Note that the applied strain value

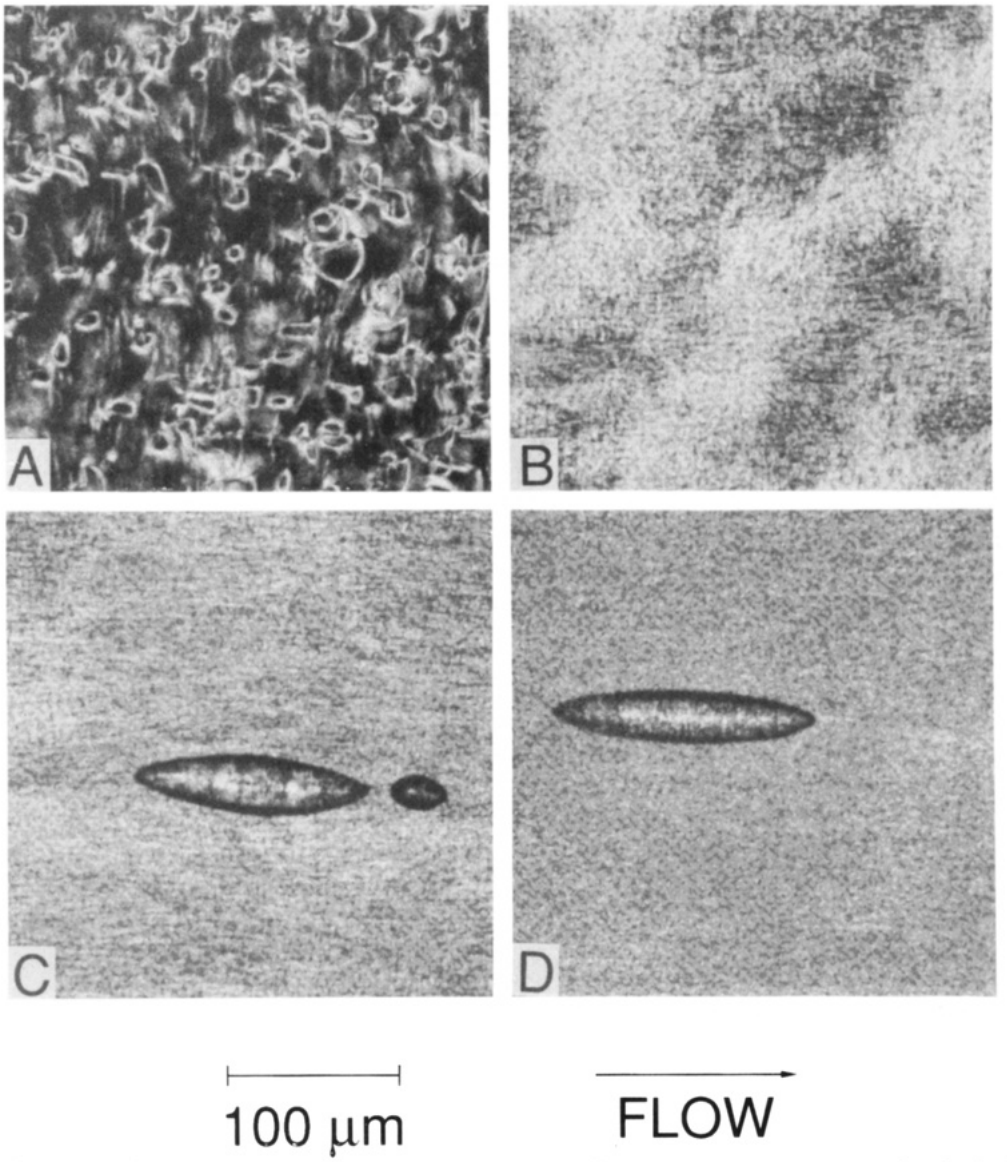

Figure 8. Optical micrographs of a 19.8% (w/w) PPTA solution at 80 °C (magnification 200×, crossed polars): (A) equilibrium structure with disclination loops; (B–D) textures during flow using $\dot{\gamma} = 5$ with strain values γt (B) 25, (C) 50, and (D) 75.

where the relative recovered strain starts to disappear ($\gamma_a = 25$) is similar to the strain at the first minimum of the transient shear stress in Figure 4.

The experiments show that beyond ~25 strain units the coherence of the structure, responsible for the elastic behavior of the solution, is destroyed.

(iii) Polarization Microscopy. To study the structural changes in more detail polarization microscopy was used. We have built a shear flow setup that can be mounted on a Leitz 350 hot stage.[7] The apparatus moves two parallel glass microscope slides at a constant speed. A gearbox provides 10 different speeds, spanning 3 decades of shear rate. The distance between the glass slides is maintained by using tungsten ribbon of a well-known thickness. The maximum strain over one complete stroke of the driving unit is 300 strain units, using 25-μm-thick tungsten spacers. For this layer thickness we can vary the shear rate between 0.5 and 500 s^{-1}.

In Figure 8A we show a texture at rest using crossed polars. This texture was obtained after ca. 15 min at rest since the last deformation of the sample. The sample is quite homogenous apart from the presence of disclination loops. These are the one-dimensional cores of the characteristic orientational defects or disclinations that can be observed in the director field of the nematic phase.[8] It should be noted that the texture shown in Figure 8A is more or less homogenously aligned due to the presence of uniform boundary conditions on the glass slides. These uniform boundary conditions are probably caused by initial preshearing of the sample during the filling of the sample cell.

In Figure 8B–D we show the texture as it develops with increasing strain (as given by $\dot{\gamma}t$). The dark objects in Figure 8C and Figure 8D are air bubbles. From Figure 8B it is observed that around 25 strain units the initially rather homogenous texture starts to change into a "dense disclination" or "grainy" texture. For more than 50 strain units relatively little change is found. The observed transition from a relatively homogenous texture at rest to a scattering dense disclination texture is not influenced by the initial texture of the sample. Samples with less uniform director alignment at rest show the same transition as a function of shear strain. A similar type of transition has been observed with thermotropic main-chain polymer liquid crystals.[9]

For large strains we observe that the "domain size" decreases with increasing shear rate. In addition, with increasing shear rate the image becomes darker, suggesting

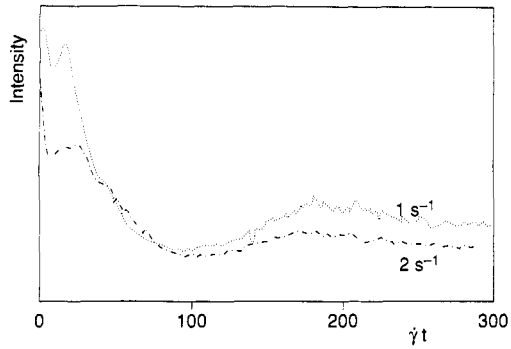

Figure 9. Transmitted light intensity using crossed polars in the Hv position as a function of applied strain for the shear rates as indicated (19.8% (w/w) PPTA, 80 °C).

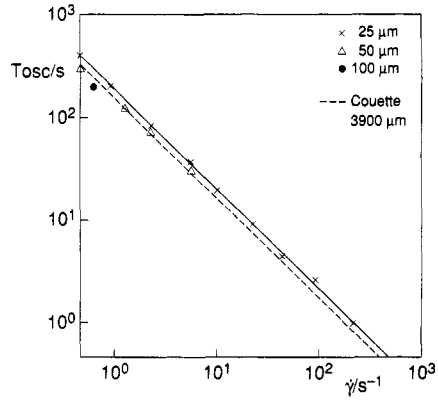

Figure 10. Oscillation time period for the transient transmitted light intensity as a function of shear rate. Thicknesses as shown: dotted line from the Couette experiments (Figure 5).

a more homogenous director field with a uniform planar alignment.

The domain size may be imagined to be a characteristic length scale for the deformation of the director field. Various definitions can (and should) be used, depending on the exact nature of the textural defects. For example, if only point disclinations were present the length scale would be given by $(1/n_0)^{1/3}$, where n_0 is the number of point disclinations per unit volume. Alternatively, a length scale λ can be defined by $\langle \cos(\beta_{\hat{n}}) \rangle = \exp(-L/\lambda)$, where $\beta_{\hat{n}}$ is the director angle at distance L. The latter definition is analogous to the definition of the persistence length of a wormlike polymer chain.

Another method to study the change in the optical texture is by measurement of the transmitted light intensity using crossed polars (in the Hv position, i.e., parallel and perpendicular to the direction of flow).[5] In Figure 9 the transmitted light intensity is shown as a function of strain for two shear rates. It is observed that the transmitted light intensity shows oscillations as a function of strain and that the period of this oscillation (defined between the first and second maximum of the transmitted light intensity) corresponds to the period that was found from the transient shear stress measurements. This is demonstrated in Figure 10 where we give the oscillation time as a function of the applied shear rate; the oscillation time is proportional to the reciprocal of the shear rate. We observe that there is apparently no effect of the layer thickness (25, 50, and 100 μm). Also the agreement with the oscillation time in the shear stress measurements (from the first to the second minimum of the transient shear stress), using a Couette geometry with a gap of 3.9 mm, is very good. This means that the oscillations in the transient shear stress are related to the

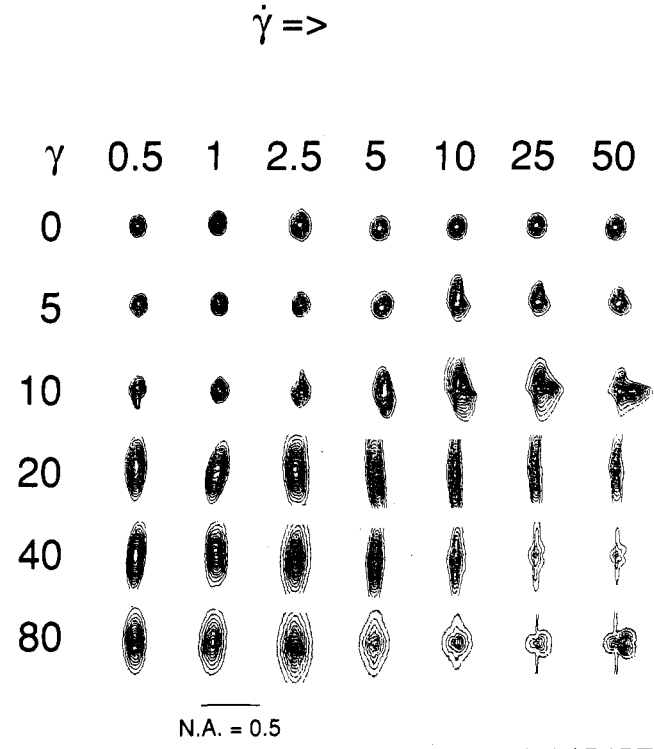

Figure 11. Conoscopic SALS Hv image of a 19.8% (w/w) DABT sample at 80 °C as a function of shear strain (γ, vertical axis) and shear rate ($\dot{\gamma}$, horizontal axis). The direction of flow was from left to right. The drawn line corresponds to a numerical aperture of 0.5; i.e., sin (θ) = 0.5, with θ the scattering angle.

change in the optical texture of the material and that there is no influence of the thickness of the sample. The oscillations in the transmitted light intensity are observed regardless of the orientation of the polars. Of course, the absolute value of the measured light intensity does depend on the orientation of the polars. We conclude that the oscillations in the transmitted light intensity and the transient shear stress are both related to the disclination density.

The oscillations in the transmitted light intensity seem to be caused by changes in scattering due to local variations of the director orientation, presumably the disclinations (or other fluctuations in the director field). One might imagine the oscillations to be caused by a complex dynamic equilibration of the disclination density from an initially low value to a higher value found for large strains. The optical texture during shear was also studied by conoscopic observation, where the back focal plane of the objective lens is observed rather than the object more or less situated at the front focal plane. If the aperture diaphragm of the condenser is closed, the incident light will strike the sample with low divergence; i.e., the incoming beam is more or less parallel. In this case the conoscopic image is similar to the SALS image in the Hv mode (polarizer and analyzer respectively parallel and perpendicular to the direction of flow). For this reason we will call this a conoscopic SALS image to differentiate from the traditional conoscopic observation where the entire aperture of the objective lens is illuminated. Traditional conoscopic observation was attempted on the sample shown in Figure 8A. However, probably due to the scattering on the remaining disclination loops, no conoscopic interference figure could be observed.

In Figure 11 we show the development of the conoscopic SALS image of a 19.8% (w/w) DABT sample at 80 °C as a function of the applied strain for various shear rates. These images were obtained by using a video camera

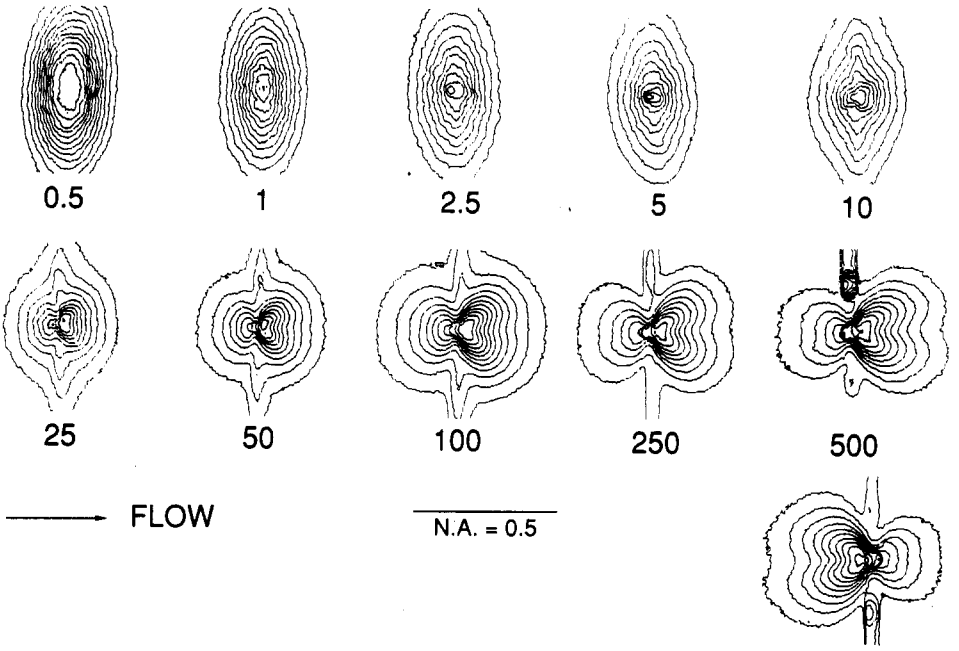

Figure 12. Conoscopic Hv (horizontal polarizer and vertical analyzer) SALS image of a 19.8% (w/w) DABT sample at 80 °C for large shear strains as a function of shear rate. The drawn line corresponds to a numerical aperture of 0.5; i.e., sin (θ) = 0.5, with θ the scattering angle.

and an image analysis system (Olympus Cue-2). A Turbo-Pascal 5.0 (Borland) program was used to calculate the contours.

We observe a structural change that is governed by the applied strain. The transition from a "defect-free" texture to a highly scattering texture seems to occur at a well-defined shear strain around 20 strain units. This strain value coincides with the value for the generation of the grainy texture from normal (orthoscopic) observation. The initial texture of the samples at rest was less uniform than shown in Figure 8A, indicating less uniform boundary conditions. However, as described before, the initial texture does not seem to have an effect on the general behavior of the sample during the start-up of flow at least as regards the generation of a dense disclination texture.

In Figure 12 we show some large-strain contour plots of the conoscopic image of a 19.8% (w/w) DABT sample. At low shear rates a rather featureless conoscopic image is observed. From the fact that no extinction takes place along the axes we conclude that the scattering objects depolarize the incident light very efficiently. With the higher shear rates we observe a different pattern that consists of a wide-angle scattering pattern and a very pronounced streak in the direction perpendicular to the direction of flow. Similar results have been reported for (hydroxypropyl)cellulose (HPC) solutions using SALS at various shear rates.[10] An interesting feature of the patterns is the asymmetry of the wide-angle pattern that reverses with reversal of the direction of flow. This is shown in Figure 12 for the highest shear rate.

The bright streak perpendicular to the direction of flow we believe is caused by the presence of stretched one-dimensional (line) disclinations. If we imagine these stretched disclinations to be highly oriented along the direction of flow, then in reciprocal space we immediately obtain a single plane perpendicular to the orientation of the disclination. In the literature the streak has been attributed to multiple defects being squeezed into elongated regions,[10] leading to a similar SALS pattern.

From experiments on 4,4′-pentylcyanobiphenyl (Merck) or 5CB, a well-known low molecular weight nematic liquid crystal, we observe that disclination loops depolarize the incident light very efficiently. In 5CB we find that between crossed polars a disclination loop is observed as a uniformly bright object, independent of the orientation of the disclination line with respect to the polars. This suggests that the highly depolarized scattered light both of the streak at high shear rates and of the elliptical scattering pattern at low shear rates can be attributed to single-line disclinations rather than the squeezed defects mentioned above.

It will be clear that one of the major problems in the quantitative interpretation of the results from polarization microscopy is the fact that the observed texture is caused by the presence of poorly defined scattering units (the disclinations). This means that the transmitted light intensity is rather difficult to calculate as it would require the knowledge of the scattering properties of a dense defect texture in an anisotropic medium. At the present time the core structure of a single disclination line is still not well understood.[11] For this reason and the likely occurrence of multiple scattering a quantitative analysis of the scattered light intensity appears to be rather intractable.

(iv) Synchrotron X-ray Scattering.[12] To obtain more unambiguous information on the structural changes in aramid solutions, we have performed X-ray scattering measurements during transient shear. The experiments were performed on a 19.8% (w/w) DABT solution in H_2SO_4 at room temperature. In the case of X-ray diffraction from solutions and melts the scattering entities are the individual molecules. By performing azimuthal scans (angle β) over the 003 meridional reflection we can measure $F(\beta)$, the experimental orientational distribution function; see Figure 13. This experimental orientational distribution was measured with a microdensitometer.

In Figure 14 we show a schematic drawing of the experimental setup, with an exploded view of the sample cell similar to that used for the polarizing microscope. There are holes in the glass slides which are covered with mica foil to allow the radiation to pass through the sample. In this case the tungsten ribbons were 50 μm thick. The exposure times using synchrotron radiation at the Daresbury Laboratory were 30 s, to be compared with at least 48 h using traditional (2 kW) X-ray generators. In

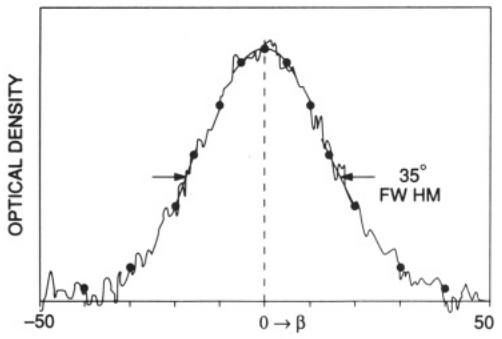

Figure 13. Example of $F(\beta)$, the experimental orientational distribution function, obtained from an azimuthal scan over the 003 meridional reflection of a 19.8% (w/w) DABT solution at 20 °C. The drawn circles are from a fit to a Maier–Saupe type curve: $F(\beta) = I_0 \exp[\alpha(P_2(\cos(\beta) - 1)]$.

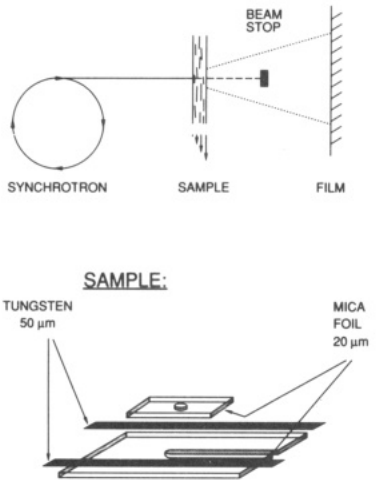

Figure 14. Experimental setup for X-ray scattering, with an exploded view of the sample cell.

combination with the time required to change films using a carrousel this leads to the possibility to expose a film every 40 s. For low shear rates it is then possible to perform transient X-ray scattering to investigate the development of orientation on the start-up of shear flow.

The experimental azimuthal half-width of the 003 meridional reflection is used to calculate an experimental order parameter S_{exp}, which is the experimental average of the $P_2(\cos(\beta))$ Legendre polynomial ($P_2(\cos(\beta)) = (1/2)[3\cos^2(\beta) - 1]$). The method to calculate S_{exp}, which is described in more detail in ref 12, is based on the observation that the experimental densitograms are described quite well by a Maier–Saupe type distribution of the form $F(\beta) = I_0 \exp[\alpha(P_2(\cos(\beta)) - 1)]$, where I_0 is the density at angle $\beta = 0$ and α is a parameter determining the width of the distribution. The parameter α is calculated from the experimental half-width assuming a Maier–Saupe type distribution. The agreement of the experimental densitogram with the Maier–Saupe distribution, using the value of α calculated from the experimental half-width, is shown in Figure 13. S_{exp} can be obtained by numerical integration using the value of α. Using this method it is possible to obtain a value for S_{exp} just by measuring the experimental azimuthal half-width, e.g., by using image analysis equipment (Olympus Cue-2) instead of using densitograms that are much more time-consuming to measure.

In the interpretation of the experimental results it is assumed that $F(\beta)$ is determined by three factors: first, the molecular orientation order with respect to the local director (described by $f(\beta')$ the molecular distribution function, where β' is the angle of a polymer chain with respect to the local director); second, the degree of lateral order of the polymer chains; and third, the macroscopic orientational order of the director field. The experimentally observed distribution function is a convolution of these contributions.

It is convenient to express the degree of molecular orientational order in terms of the $\langle P_2 \rangle$ order parameter, where the brackets indicate a molecular average of $P_2(\cos(\beta'))$. $\langle P_2 \rangle$ is euqal to 1 for perfect molecular alignment and $\langle P_2 \rangle$ is equal to zero if no orientational order is present, i.e., for the isotropic phase. Similarly, we define the degree of director alignment by $\bar{P}_2$, where the bar indicates an average of $P_2(\cos(\beta_{\hat{n}}))$ taken over the director field orientation angle $\beta_{\hat{n}}$. Using the definitions given above we will write the experimental order parameter S_{exp} as a product of three contributions:[13]

$$S_{exp} = K\langle P_2 \rangle \bar{P}_2 \tag{2}$$

where $\langle P_2 \rangle$ is the molecular order parameter, $\bar{P}_2$ is the director order parameter, and K is an unknown factor due to the lateral disorder of the polymer chains. The decomposition in eq 2 is based on the closure relation for Wigner matrices (generalized spherical harmonics). In the case of a convolution of two uniaxial orientational distributions this reduces to taking the product of the corresponding Legendre coefficients in the Legendre series expansions of the distributions. This procedure is analogous to the rule for performing a convolution using Fourier series expansion. The factor K in eq 2 is the "apparent order parameter" that would be found for a perfectly aligned sample (both molecular and director order parameters equal to one) where the width of the meridional reflections is determined by the degree of lateral correlation of the polymer chains along the c axis.[14] For the case of no lateral correlation the meridional reflections would be broad layer lines corresponding to the Fourier transform of an individual polymer chain, and for the case of perfect lateral correlation the meridional reflections would be sharp spots (both cases in the absence of orientational disorder). The unknown degree of lateral correlation in these aramid solutions thus leads to an unknown additional broadening of the meridional reflections. This experimental effect can in principle be avoided by using the equatorial reflections instead. However, the equatorial reflections are much weaker than the meridional reflections so that no accurate values are availabe.

As mentioned above, in eq 2 we are implicitly assuming uniaxial symmetry both at a molecular and at a macroscopic level. If we now also assume that the local molecular order, both orientational and lateral, is independent of the application of an external flow field, then the experimental order parameter from X-ray scattering is proportional to the director order parameter $\bar{P}_2$. This means that we are assuming that $K\langle P_2 \rangle$ is constant. It is not to be expected that the local molecular order $\langle P_2 \rangle$ can be influenced to any extent by external flow fields. This is due to the fact that the molecular orientational order is very high already, so that the moment applied on the molecules by a velocity gradient will be small. Of course for systems close to the nematic–isotropic transition this assumption is not valid as has been observed experimentally from the flow-induced birefringence in the isotropic phase.[3]

In Figure 15 we present some results for S_{exp} as a function of the applied strain (averaged over the exposure time interval of the film). Two regions are observed: up to a strain of about 25 a steadily increasing orientation, and

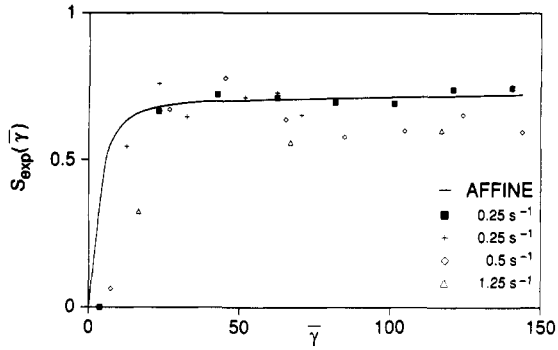

Figure 15. Experimental order parameters S_{exp} as a function of the average applied strain during the exposure of the film (19.8% (w/w) DABT, 20 °C).

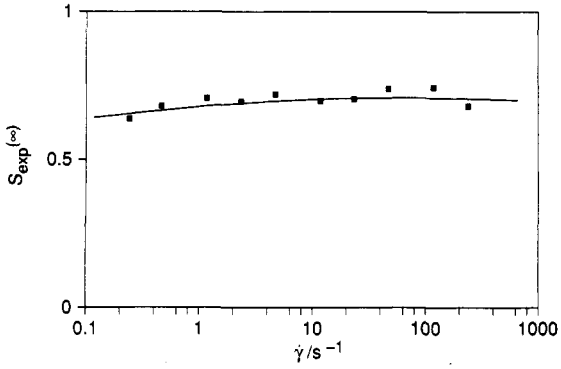

Figure 16. Large-strain value for the experimental order parameter $S_{exp}(\infty)$ as a function of shear rate (19.8% (w/w) DABT, 20 °C).

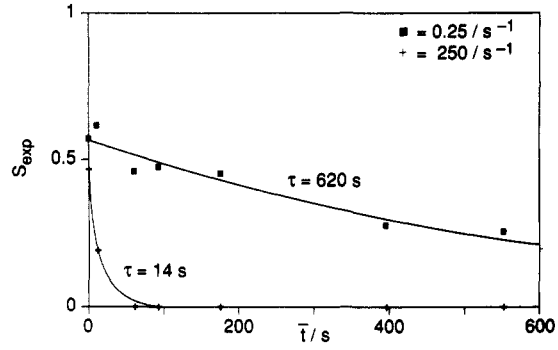

Figure 17. Orientation relaxation after large strain at the indicated shear rates as a function of the average time after cessation of flow (19.8% (w/w) DABT, 20 °C).

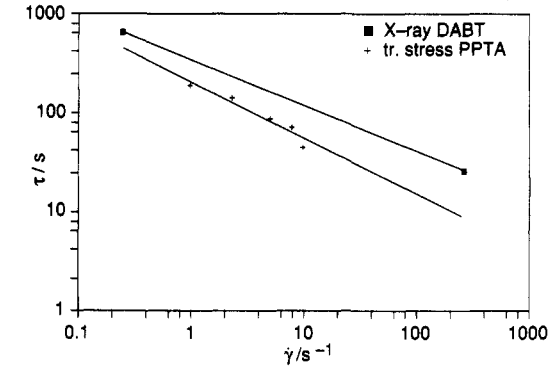

Figure 18. Structure relaxation times from X-ray scattering (19.8% (w/w) DABT, 20 °C) and intermittent shear-step experiments (19.8% (w/w) PPTA, 80 °C) for a large prestrain as a function of preshear rate.

for larger strains a saturation to a constant value. The orientation process is mainly determined by the applied strain. In Figure 16 we show the ultimate, large-strain, value $S_{exp}(\infty)$ as a function of shear rate. We observe that there is only a very slight influence of the shear rate on $S_{exp}(\infty)$, the steady-state orientational order. This steady-state value we feel must coincide with the case of perfect director alignment ($\bar{P}_2 = 1$) along the direction of flow. Also the slight influence of the shear rate on $S_{exp}(\infty)$ indicates that the separation of the orientational order into factors related to the molecular order ($K\langle P_2\rangle$) and a factor determined by the orientational order of the director field ($\bar{P}_2$) is a reasonable approximation. That the average director orientation is along the direction of flow is also confirmed by X-ray scattering on manually sheared and coagulated PPTA films. By performing X-ray scattering at various angles of incidence, we conclude that the average molecular orientation is along the direction of flow; i.e., the flow alignment angle describing the tilt of the director in simple shear flow is about 0°.

From the measured value of $S_{exp}(\infty)$ and the value for $\langle P_2\rangle$ of about 0.92–0.95 that is expected from modulus values of as-spun fibers and from a simple mean-field-like theory that has been developed for lyotropic nematic liquid crystals, we conclude that the broadening of the meridional reflections due to local lateral (dis)order is indeed an important factor with $K \simeq 0.73/\langle P_2\rangle = 0.78$. This value can be compared to a value for K obtained by visually determining the ratio of the azimuthal half-widths of the 003 meridional and the weak equatorial reflection. From the measured ratio we find $K = 0.82 \pm 0.05$, in reasonable agreement with the value given above.

It is observed that the required strain for the saturation of the orientation order seems to coincide with the first minimum of the transient shear stres, the decay of the relative recovered strain in the recoil experiments, and the generation of the dense disclination texture in polarization microscopy.

By calculating the effect of a simple affine deformation model on an initially random director field, we obtain the drawn curve in Figure 15, where the case $\bar{P}_2 = 1$ corresponds to the large-strain value $S_{exp}(\infty)$. From this we conclude that the development of the orientational order in the director field is adequately explained by an affine deformation model. The affine deformation model is briefly described in the Appendix; for more details, see ref 12.

(v) Structure Relaxation Experiments. To study the relaxation of the shear-flow-induced structure we have performed two measurements. The first is to measure the decay of the experimental order parameter S_{exp} after cessation of flow, and the second is the measurement of the second transient of the transient shear stress after a certain time since the application of the first strain.

In Figure 17 we show the results of orientation relaxation experiments, where the flow is stopped at time $t = 0$ and the relaxation of the experimental order parameter is measured, for two preshear rates. In both cases the applied prestrain was large, so that the equilibrium structure during shear flow was reached. The points at $t = 0$ correspond to the value of S_{exp} just before the cessation of flow. The time shown on the ordinate is the average time since the cessation of flow, and the order parameter is an average over the time interval required for the exposure of the film. For the two preshear rates it is observed that the corresponding relaxation times τ differ widely. These relaxation times are shown in Figure 18.

In Figure 19 we show an intermittent shear-step experiment. The first transient is from an equilibrium structure, and the second transient is after a certain pause time t_p. It is seen that the amplitude of the second

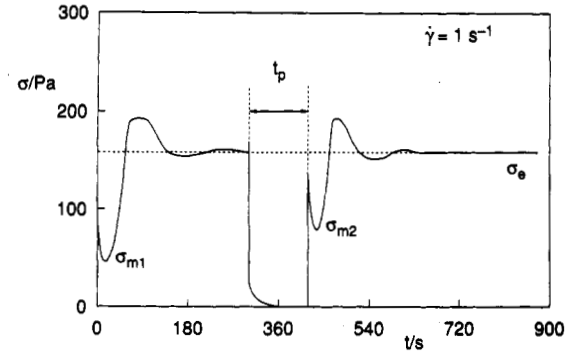

Figure 19. Intermittent shear-step experiment on 19.8% (w/w) PPTA at 80 °C: first transient from an equilibrium structure; second transient after pause time t_p. The relative amplitude of the second transient is a measure for the relaxation of the large-strain steady-state structure at the end of the first strain.

transient is less than that of the first one. The amplitude of the second transient will depend on the pause time t_p, so that by studying the relative amplitude of the second transient as a function of the pause time, we can obtain a "structure relaxation time". The relative amplitude of the second transient is given by the recovery function $R(t_p)$:

$$R(t_p) = \frac{\sigma_{m2} - \sigma_e}{\sigma_{m1} - \sigma_e} \equiv \tanh\left(\left(\frac{t_p}{\tau}\right)^{\alpha}\right) \qquad (3)$$

Here, τ is a characteristic time constant for the relaxation process, and α is an additional parameter. It is stressed that the formula for the recovery function given in eq 3 is purely empirical and was obtained by a trial and error method. The values of τ obtained with eq 3 are shown in Figure 18.

There is quite reasonable agreement between the X-ray data and the intermittent shear-step results, especially since the X-ray measurements were done on a DABT solution at room temperature and the intermittent shear-step measurements were performed on a PPTA solution at 80 °C.

Discussion

In the experimental section several methods were described to study the change in the structure of aramid solution during the start-up of simple shear flow. Here we will attempt to combine the various experimental observations into one consistent qualitative model for the structure and rheology of aramid solutions. We note that this qualitative model is only intended as a starting point for discussion and is not intended to be rigorous in any way.

The synchrotron X-ray scattering experiments indicate that during the start-up of simple shear flow we are effectively dealing with an affine deformation of the director field. The other start-up experiments all show a strain dependence of the start-up behavior in support of this affine deformation hypothesis. In all the experiments a critical strain on the order of 20–25 strain units seem to be an important number. We observe that such a value is in reasonable agreement with the leveling off of the director orientation calculated with the affine deformation model (see Appendix).

From the measurements with synchrotron X-ray scattering we also conclude that the overall average order in the director field for large shear strains is more or less independent of the shear rate from 0.25 to 250 s^{-1}. This indicates that the $\bar{P}_2$ director order parameter is close to 1 for large strains, independent of shear rate. A value substantially less than 1 we feel would be inconsistent with the observation that it is easy to make highly oriented aramid films by applying shear to a solution and subsequently coagulating in water. The degree of molecular alignment with respect to shear direction is in the same order as that found in aramid fibers; i.e., $S_{exp} = 0.95$ (obtained using the 110 and 200 equatorial reflections).

From the above arguments we arrive at a simple model for the start-up of shear flow where the average director orientation is described by affine deformation and where for large strains the director orientation is essentially perfect irrespective of shear rate. The observation that the relative recovered strain for small prestrains is about 70% indicates that there is some "slippage".

Apart from the overall average of the director orientation as described above, it is of interest to consider the optical image obtained with polarization microscopy and the conoscopic SALS results. Initially, the "tumbling domain" type flow that is visually observed during simple shear led us to believe that the director orientation is far from perfect using this geometry. However, the results of the X-ray scattering indicate that an, on average, well-aligned director field can apparently contain a substantial amount of disclinations that lead to the observed image of "domains". If we follow this line of reasoning we are forced to conclude that the disclinations, which are either point or line singularities, do not occupy a substantial volume fraction of the sample. This disclination gas type of description of simple shear flow can explain several experimental observations.

Initially, relatively few disclination loops are found; see Figure 8A. Then after application of several strain units, the one-dimensional disclinations will be rotated and stretched by the affine simple-shear deformation along with the rest of the director field.

Although it is not easy to calculate an exact expression for the energy, it is relatively easy to see that the stretching of a one-dimensional disclination loop will lead to an increase of the elastic energy stored in the director field. The energy of a single disclination line is given by[11]

$$E_{el} = LK_e m^2 \ln(\rho_{max}/a_m) + LE_c \qquad (4)$$

where L is the length of the disclination, K_e is an elastic constant related to one or several of the Frank elastic constants, m is the order of the disclination (i.e., traversing a closed contour around the disclination line will lead to the director rotating over $2m\pi$ radians), ρ_{max} is the radius of the cylindrical region affected by the presence of the disclination, a_m is the core radius of the disclination, and E_c is an unknown energy required to generate the core of the disclination. The important information from eq 4 is that the energy stored in a line defect is proportional to the length of the core of the line. This means that we may imagine the disclination gas to consist of "elastic springs" where the stored energy is linear with the deformation rather than quadratic as follows from Hook's law for traditional elasticity.

With this concept of energy stored in the disclination loops, the experimentally observed generation of additional disclinations resembles elastic fracture of a solid. Above a certain strain part of the elastically stored energy is used for the formation of additional disclinations. At this strain level the disclination loops break up into many smaller loops.

By visual observation the generation of defects seems to be a nucleation and growth type of process; new disclinations are formed both around the initially present disclinations and in homogenously aligned defect-free regions. Around 20 strain units "clouds of disclination

loops" can be observed that seem to collide, grow, and sometimes even disappear or annihilate each other. Such clouds can be observed in Figure 8B.

The observation that the elastic recoil strain decreases beyond about 20 prestrain units (Figure 7) is in agreement with the disclination gas model given above where the coherence in the structure is destroyed once the disclination loops fall apart into smaller loops. Also, the conoscopic image at higher shear rates shows the presence of one-dimensional scattering units oriented in the direction of flow. We believe that these scattering units are the stretched disclination loops.

It is more difficult to explain the oscillations that are observed in the transient shear stress (Figure 4). Presumably, the oscillations in the transient shear stress are related in some way to the "disclination gas". This follows from the observation that the oscillations in the transmitted light intensity have the same period as the transients in the shear stress and the fact that the oscillations in the transmitted light intensity are observed irrespective of the use of polars. The latter implies that the oscillations are mainly related to the turbidity of the sample or the "disclination density". We do not have an explanation for the occurrence of a damped oscillation. However, it would seem to be reasonable to assume that the oscillations in the transmitted light intensity and the transient shear stress are both caused by the disclination gas attempting to reach a steady-state situation but where apparently overshoot occurs. Possibly the number of defects formed around 20 strain units is larger than the steady-state value so that subsequent annealing takes place and an equilibrium between "disclination creation" and "disclination annihilation" has to be found.

Also, the structure relaxation times as found from X-ray scattering and intermittent shear experiments require further thought. Possibly the occurrence of slippage of the disclination loops is less at higher shear rates, leading to a more rapid destruction of the director orientation as the loops contract after cessation of flow.

This contraction process we believe is also responsible for the well-known "banded texture" that is observed after cessation of flow at higher shear rates. From the conoscopic images we are confident that banded textures do not occur during flow. After the cessation of a high shear rate deformation a backflow can be observed that appears to be related to the generation of the banded textures. In the literature it has been reported that actual occurrence of banded textures is also governed by the amount of prestrain.[10] This result is possibly related to the required strain for the sample to change from an affinity deformed to a dense disclination texture.

In conclusion we believe that during the start-up of simple-shear flow the following takes place (at least in aramid solutions and probably in other lyotropic nematic materials such PBLG and HPC): first, that up to a strain of about 20 an affine deformation of the initial texture takes place, leading to an, on average, highly oriented director field; second, that beyond the initial 20 strain units the elastic energy that is stored, e.g., in the initially present disclinations, is partially used for the formation of additional disclinations and/or the breaking up of the already present disclinations; third, that the equilibration process of the "disclination gas" causes the oscillations in the transient shear stress and in the transmitted light intensity.

Although the model given above is highly speculative, we feel that some of the experimental observations are at least qualitatively explained. It will be obvious that still much work has to be done to test and justify the various details of the model.

Acknowledgment. We thank Dr. Ir. J. J. van Aartsen and Prof. H. N. W. Lekkerkerker for stimulating discussions and their continued interest in this work. The assistance provided by the personnel at the Daresbury Laboratory was much appreciated. We also thank Ing. A. Schaap of the Fiber Physics Department (Akzo Fibres and Polymers Division) for his assistance with the image analysis.

Appendix[12]

To calculate the orientation due to a simple shear deformation the following affine deformation model was used. It should be noted that an affine deformation model gives the highest possible degree of orientation due to the absence of any slip.

A simple shear deformation is conveniently described by the deformation tensor F_j^i, where

$$x_j' = F_j^i x_i$$

and on an orthonormal coordinate system it holds

$$F_j^i = \begin{bmatrix} 1 & 0 & 0 \\ 0 & 1 & 0 \\ \gamma & 0 & 1 \end{bmatrix}$$

The orientational distribution is calculated as a function of the shear strain γ using a statistical method. Unlike an elongational deformation, where the symmetry axis is well defined and simple analysis can be used, the analytical calculation of the orientational distribution function and order parameters for a simple shear deformation appears to be rather complicated.

The statistical method is as follows: (i) generate a random unit vector from an isotropic orientational distribution (φ from $[0,2\pi]$ and cos (θ) from $[1,-1]$); (ii) transform this vector using $F_j^i(\gamma)$; (iii) calculate the polar angles φ' and θ' and appropriate order parameters such as $P_2(\cos(\theta')) = (1/2)(3\cos^2(\theta') - 1)$ and $D = (3/2)\sin^2(\theta')\cos(2\varphi')$; (iv) set $N = N + 1$; (v) if $N < N_{max}$ goto i.

From the set of values of P_2 and D averages can be calculated for each shear strain γ. In Figure 20 the results are shown for $\bar{P}_2$, the orientational order parameter, and $\bar{D}$, the biaxiality parameter. These order parameters can be calculated by using the following analytic approximations:

$$\bar{P}_2(\gamma) = \left[1 - \frac{3\gamma}{2\gamma^2 + 90}\right]\left[\frac{\gamma^2}{\gamma^2 + 6}\right]$$

$$D(\gamma) = \frac{\gamma(1 - \exp(-3/2\gamma))}{\gamma + 10(1 - \exp(-3/2\gamma))}$$

The accuracy of these approximations over the whole strain range can be seen in Figure 20.

In Figure 20 we also show the result for an elongation deformation as a function of γ ($a = 1 + \gamma$, $x' = x/a^{1/2}$, $y' = y/a^{1/2}$, $z' = za$). This is given by the Kuhn and Grün equation:[15]

$$\bar{P}_2(a) = \frac{2a^3 + 1}{2(a^3 - 1)} - \frac{3a^3}{2(a^3 - 1)^{3/2}}\arctan((a^3 - 1)^{1/2})$$

Of course, for an elongation deformation $\bar{D} = 0$ from symmetry arguments. It is observed that an elongational deformation provides a much more efficient orientation than a simple shear deformation.

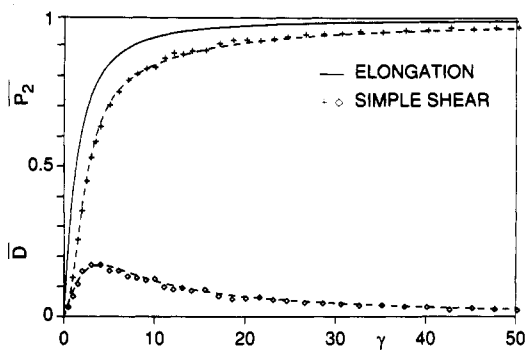

Figure 20. Director orientational order parameters $\bar{P}_2$ (+) and $\bar{D}$ (◇) obtained from the affine deformation model for simple shear together with the result for elongation using the Kuhn and Grün equation (drawn curve). The dashed curves are from the analytic approximations given in the Appendix.

The stronger γ dependence for an elongation deformation explains the rather poor reputation of shear deformation for the formation of high-modulus materials. One conclusion of these calculations is that if sufficient strain can be applied the degree of orientation due to simple shear can be just as high as that obtained from elongation, although in practice applying a shear strain of about 40 is often not possible.

References and Notes

(1) Picken, S. J. *Macromolecules* **1989**, *22*, 1766.
(2) Picken, S. J. *Macromolecules* **1990**, *23*, 464.
(3) Picken, S. J. *Liq. Cryst.* **1989**, *5*, 1635.
(4) Berry, G. C. *Mol. Cryst. Liq. Cryst.* **1988**, *165*, 333.
(5) Doppert, H. L.; Picken, S. J. *Mol. Cryst. Liq. Cryst.* **1987**, *153*, 109.
(6) Moldenaers, P.; Mewis, J. *Proc. World Congr. III Chem. Eng.* **1986**, *4*, 546.
(7) Blok, P.; Picken, S. J.; Verwaaien, H. H. T. *Constructeur* **1987**, *26* (12), 44 (in Dutch).
(8) Frank, F. C. *Discuss. Faraday Soc.* **1958**, *25*, 19.
(9) Alderman, N. J.; Mackley, M. R. *Faraday Discuss. Chem. Soc.* **1985**, *79*, 149.
(10) Ernst, B.; Navard, P. *Macromolecules* **1989**, *22*, 1419.
(11) Vertogen, G.; de Jeu, W. H. *Thermotropic Liquid Crystals: Fundamentals*; Springer-Verlag: Berlin, 1988.
(12) Picken, S. J.; Aerts, J.; Visser, R.; Northolt, M. G. *Macromolecules* **1990**, *23*, 3849.
(13) Zannoni, C. Distribution Functions and Order Parameters. In *The Molecular Physics of Liquid Crystals*; Luckhurst, G. R., Gray, G. W., Eds.; Academic Press: New York, 1979, Chapter 3.
(14) Vainshtein, B. K. *Diffraction of X-rays by Chain Molecules*; Elsevier: Amsterdam, 1966; Chapter IV, pp 274–281.
(15) Kuhn, W.; Grün, F. *Kolloid-Z.* **1942**, *101*, 248.

Registry No. PPTA (copolymer), 25035-37-4; PPTA (SRU), 24938-64-5; DABT (copolymer), 29153-47-7; DABT (SRU), 108773-35-9.